



HAL
open science

Nonlinear dynamics of directional drilling with fluid and borehole interactions

Quang-Think Tran, Khac-Long Nguyen, Lionel Manin, Marie-Ange Andrianoely, Régis Dufour, Mohamed Mahjoub, Stephane Menand

► **To cite this version:**

Quang-Think Tran, Khac-Long Nguyen, Lionel Manin, Marie-Ange Andrianoely, Régis Dufour, et al.. Nonlinear dynamics of directional drilling with fluid and borehole interactions. *Journal of Sound and Vibration*, 2019, 462, pp.114924. 10.1016/j.jsv.2019.114924 . hal-02297671

HAL Id: hal-02297671

<https://hal.science/hal-02297671>

Submitted on 21 Dec 2021

HAL is a multi-disciplinary open access archive for the deposit and dissemination of scientific research documents, whether they are published or not. The documents may come from teaching and research institutions in France or abroad, or from public or private research centers.

L'archive ouverte pluridisciplinaire **HAL**, est destinée au dépôt et à la diffusion de documents scientifiques de niveau recherche, publiés ou non, émanant des établissements d'enseignement et de recherche français ou étrangers, des laboratoires publics ou privés.



Distributed under a Creative Commons Attribution - NonCommercial 4.0 International License

Nonlinear dynamics of directional drilling with fluid and borehole interactions

Quang-Thinh Tran^{a,*}, Khac-Long Nguyen^a, Lionel Manin^a, Marie-Ange Andrianoely^a, Régis Dufour^a, Mohamed Mahjoub^b, Stéphane Menand^b

^aUniv Lyon, INSA-Lyon, CNRS UMR5259, LaMCoS, F-69621, France

^bDrillScan, 69100 Villeurbanne, France

Abstract

In rotary drilling, a drillstring is an assembly of slender pipes. It is used to transmit the driving torque of a motor at the drilling surface to the drill bit at the bottom hole of a 3D well. Numerous vibratory phenomena are induced during the drilling: whirling, stick-slip, bit-bouncing, lateral instability, inducing in particular reduction of the rate of penetration and mean time between failures. For the rotordynamics prediction of such a structure, the drillpipes are modelled with Timoshenko beam elements, containing 12 degrees of freedom, equipped with distributed radial stop-ends. The rotary motion is assumed to have a constant speed of rotation imposed at the top of the drillstring. The drilling mud is taken into account by using a fluid-structure interaction model. The numerical simulations concern a real 3D-borehole and a parametric analysis is carried out for determining the role of the mud density and of the flows rate on the drillstring dynamics. **It is shown that increasing the flow rate and densifying the drilling fluid reduce the fluid damping effect that increases drillstring lateral vibrations.**

Keywords: rotary drilling, fluid-structure interaction, drillstring dynamics, drillstring-borehole contact, stick-slip, rotordynamics

1. Introduction

Basically, rotary geothermic or oil drilling has a 3D curved well trajectory, carried out by using a very long drillstring made of slender pipes and a tool bit, running in a 60-120 rpm speed of rotation range. The lowest component of the drillstring so-called the bottom hole assembly (BHA) consists of heavyweight drill pipes whose weight on the bit makes possible the rate of penetration (ROP). The mud plays the role of a drilling fluid: rock-cutting evacuation, cooling and lubrication. It is pumped downward inside the drillpipe and upward in the annular space between the drillpipe and the well. During the drilling, the unbalance masses distributed along the drillstring, the mud pumping, and the excitation generated by the drill bit induce drillstring vibrations combining lateral, torsional and longitudinal motions, triggering non expected phenomena such as forward and backward whirlings, stick-slip, bit-bouncing [1, 2, 3, 4]. This set of phenomena is detrimental to the proper drilling operation and can lead to: equipment failures, reduction of the mean time between failures and of the ROP.

In order to avoid such adverse dynamic phenomena, it is required to understand, to predict and to control the drilling dynamics which is a complex rotordynamics problem. For this purpose, a proper model has to take into account several drilling-related specific features such as the preloaded slender rotating string immersed in a 3D well, the eccentricity of the drillstring in the well, the numerous drillpipe - borehole contacts, the fluid-structure interaction, the motion couplings, the parametric excitation due to the weight on bit (WOB) and torque on bit (TOB).

Fluid-structure interactions have been investigated since a few decades in the literature. Chen et al. [5], studied the vibration of a rod confined in Newtonian fluid, the fluid effects being considered by the hydrodynamic forces which contain the added mass and damping coefficients. The similar formulations for fluid-related coefficients proposed in [5] are utilized in the thesis of Shyu [6] for different types of fluid. Heisig [7] computed the eigenfrequencies

*Corresponding author

Email address: quang-thinh.tran@insa-lyon.fr (Quang-Thinh Tran)

by analytical formulas dedicated to a drillstring confined in a horizontal extended well and taking into account the inertial effect through added mass coefficients provided in [8], but not the damping effect. Numerical and experimental investigations about the effect of fluid on rotor in bending were carried out by Axisa and Antunes [9, 10]. The fluid force was interpreted by three effects which depend on the fluid characteristics: inertia, friction, and viscosity. Except the added mass matrix derived from inertial effect, the stiffness and damping matrices related to fluid were expressed as function of the speed of rotation. In their extended research, Antunes et al. [11] expressed the hydrodynamic force in terms of annular space eccentricity. Khulief et al. [12] studied the fluid elastic effects on the drillstring vibrations based on the model presented in [11] with a fluid friction coefficient **adjusted** experimentally. However these works did not consider the upward and downward mud flows.

Paidoussis et al. [13] investigated the dynamic behavior of a cantilever pipe by considering the inside and outside fluid flows. This model was used to simulate the vibration of a drillstring immersed in drilling mud in subsequent works [14, 15, 16, 17]. Zhang et al. [18] used the same model to determine the critical flow rate for the buckling of a nonrotating drillpipe conveying fluid. **However in these aforementioned studies, the drillstring dynamics is analyzed only for straight wells, either vertical or horizontal.** In practice, the drilling is directional leading to a deviated well trajectory. Feng et al. [19] considered the profile of the well in their dynamic analysis of a directional drillstring but neglected the mud. **Recently, in [20] Feng et al. continued this investigation by using a planar curved finite element (FE) beam.**

The model presented hereafter focuses on the dynamic behavior of the drillstring taking into account the mud - drillstring interaction and the drillstring - borehole contacts. The FE model including contact forces, mass unbalance and fluid - drillstring interactions is presented in Section 2. Section 3 is dedicated to the dynamic computation procedure. In Section 4, the influence of the fluid on the drillstring vibration is discussed. Finally, conclusions are drawn in Section 5

Nomenclature

A_i, A_o drillstring inner and outer cross-sections [m^2]

C_c, c_c contact damping and its maximum value [Ns/m]

C_f viscous damping coefficient

D_o drillstring outer diameter [m]

D_{ch} borehole inner diameter [m]

F_0^e elementary axial force [N]

F_A lateral hydrodynamic inviscible force per unit length [N/m]

F_L, F_N drilling fluid frictional forces due to the annular flow in longitudinal and normal directions per unit length [N/m]

F_{axial} axial force [N]

F_{en}, F_{et} fluid forces due to external flow in normal and tangent directions [N/m]

F_{fx}, F_{fy}, F_{fz} fluid forces per unit length acting on drillstring element in local frame [N/m]

F_{in}, F_{it} fluid forces due to internal flow in normal and tangent directions [N/m]

F_{pz}, F_{pr} longitudinal and radial pressure forces per unit length [N/m]

G_e shear modulus [N/m^2]

I_e, I_p^e beam element flexural and polar moments [m^4]

K_c, k_c contact stiffness and its maximum value [N/m]

	M_d	drillstring total mass [kg]
	M_t, M_f	drillstring and drilling fluid masses per unit length [kg/m]
	M_u	total mass unbalance [g.mm]
	P	penetration [m]
65	Q	transversal shear force [N]
	Q_f	drilling fluid flow rate [m ³ /s]
	R_e	drillstring outer radius [m]
	S	Stokes number
	S_e	beam element cross-section [m ²]
70	S_r^e	cross-section reduced area [m ²]
	T	elementary kinetic energies of the drillstring [J]
	TOB	torque-on-bit [N]
	T_0^e	elementary axial torque [Nm]
	T_u	kinetic energy of a discrete unbalance mass [J]
75	U	elementary strain energy [J]
	U_i, U_o	downward and upward mean velocities of the drilling fluid inside and outside the drillstring [m/s]
	$U_{F_0^c}$	strain energy due to the axial force [J]
	WOB	weight-on-bit [N]
	Ω	speed of rotation imposed to the drillstring [rad/s]
80	α, β	Rayleigh damping coefficients [s ⁻¹], [s]
	α_u	initial angular position of the mass unbalance [rad]
	C_f	damping matrix of the drilling fluid [Ns/m]
	C	damping and Coriolis matrices of drillstring [Ns/m, Ns/rad]
	F_c^{qs}	quasi-static contact force vector [N]
85	F_c	contact force vector [N]
	F_s	static force vector [N]
	F_u	centrifugal force vector [N]
	F_{cn}^{qs}, F_{ct}^{qs}	quasi-static normal and tangential contact forces vectors [N]
	F_{cn}, F_{ct}	normal and frictional contact forces vectors [N]
90	K_g	drillstring geometric stiffness matrix [N/m, N/rad]
	K, K_f	drillstring and drilling fluid stiffness matrices [N/m, N/rad]
	M, M_f	drillstring and drilling fluid mass matrices [kg, kgm ² /rad]

	N	shape functions matrix
	T_f	frictional contact torque vector [Nm]
95	T_f^{qs}	quasi-static contact torque vector [Nm]
	$\delta_e, \delta_n, \delta$	elementary, nodal and total dof vectors [m, rad]
	$\omega_{R_1/R}^{R_1}$	instantaneous angular velocity vector of R_1 frame [rad/s]
	f_f^x, f_f^y, f_f^z	elementary forces vectors of the drilling fluid in local frame [N]
	χ	added mass coefficient
100	δW	virtual work associated with the axial torque [J]
	\dot{x}	time derivation of x
	ϵ_{zz}^{nl}	nonlinear terms of deformation field
	γ	angle between tangential vectors of the drillstring center line in undeformed and deformed states [rad]
	λ_k, λ_c	regularized parameters [m^{-1}]
105	$[C_e]^f$	elementary Coriolis matrix of the drilling fluid [Ns/m]
	$[K_e]^f$	elementary stiffness matrix of the drilling fluid [N/m]
	$[M_e]^f$	elementary mass matrix of the drilling fluid [kg]
	μ	friction coefficient
	μ_s, μ_d	static and dynamic friction coefficients
110	ν_f	apparent kinematic viscosity of drilling fluid [m^2/s]
	$\vec{I}, \vec{J}, \vec{K}$	unit vectors of the global frame
	$\vec{i}, \vec{j}, \vec{k}$	unit vectors of the local frame
	\vec{n}, \vec{t}	unit normal and tangent vectors
	ψ, θ, ϕ	rotational angles of the rotation matrix of the global-local frames transformation [rad]
115	ρ_e, ρ_f	beam element and drilling fluid density [kg/m^3]
	θ_x, θ_y, Φ	rotational angles of the rotation matrix of the undeformed-deformed frames transformation [rad]
	θ_z	twist angle [rad]
	a	shear effect coefficient
	a_t	drillstring lateral acceleration in the local frame [m/s^2]
120	a_{fx}, a_{fy}, a_{fz}	drilling fluid accelerations in the local frame [m/s^2]
	d	gyration radius [m]
	j_0	drillstring borehole clearance [m]
	k	damping coefficient of drilling fluid [Ns/m]

	l_e	beam element length [m]
125	m_u	unbalance mass [kg]
	p_i, p_o	drilling fluid pressures inside and outside the drillstring [Pa]
	r	radial displacement [m]
	t	time [s]
	v_g	sliding speed velocity of drillstring on the borehole wall [m/s]
130	v_{ref}	reference velocity [m/s]

2. 3D Beam Finite Element model

2.1. Coordinate system definition

The FE formulation of the drillstring dynamic model is carried out in a curved borehole. Let the frame of reference $OXYZ$ be Galilean, and $Axyz$ be the local frame of reference linked to the drillstring, see Fig.1. The rotation matrix

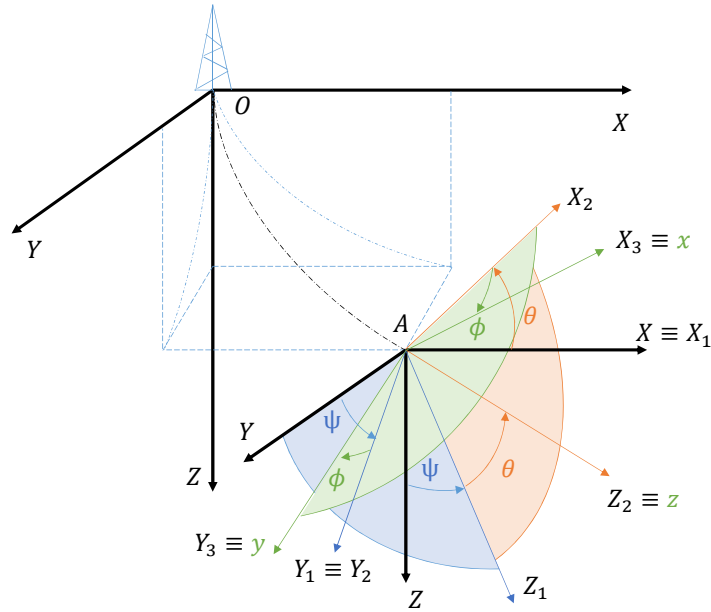


Figure 1: Transformation from global to local coordinates

from global to local coordinates is established with the three rotations ψ around X , θ around Y_1 and ϕ around Z_2 .

$$\begin{pmatrix} \vec{I} \\ \vec{J} \\ \vec{K} \end{pmatrix} = \begin{bmatrix} \cos \theta \cos \phi & -\cos \theta \sin \phi & \sin \theta \\ \sin \psi \sin \theta \cos \phi + \cos \psi \sin \phi & -\sin \psi \sin \theta \sin \phi + \cos \psi \cos \phi & -\sin \psi \cos \phi \\ -\cos \psi \sin \theta \cos \phi + \sin \psi \sin \phi & \cos \psi \sin \theta \sin \phi + \sin \psi \cos \phi & \cos \psi \cos \theta \end{bmatrix} \begin{pmatrix} \vec{i} \\ \vec{j} \\ \vec{k} \end{pmatrix} \quad (1)$$

where $(\vec{I}, \vec{J}, \vec{K})$ and $(\vec{i}, \vec{j}, \vec{k})$ are the unit vectors of the global and local coordinate systems, respectively. In the undeformed state, the drillstring is located at the center line of the well $(R)Axyz$. The frame $(R_1)Ax_1y_1z_1$ is linked to

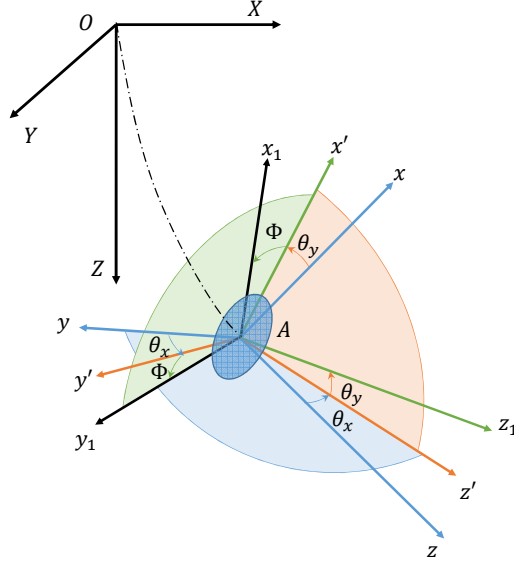


Figure 2: Transformation from undeformed to deformed states

the drillstring center line during its vibration. **The transformation from the undeformed state to the deformed state of the drillstring is carried out using a set of three rotation angles θ_x , θ_y , Φ about x , y' and z_1 axis, respectively, see Fig.2.** The instantaneous angular velocity vector of the R_1 frame is:

$$\omega_{R_1/R}^{R_1} = \begin{bmatrix} \omega_x \\ \omega_y \\ \omega_z \end{bmatrix} = \begin{bmatrix} \dot{\theta}_x \cos \theta_y \cos \Phi + \dot{\theta}_y \sin \Phi \\ -\dot{\theta}_x \cos \theta_y \sin \Phi + \dot{\theta}_y \cos \Phi \\ \dot{\Phi} + \dot{\theta}_x \sin \theta_y \end{bmatrix} \quad (2)$$

with $\Phi = \Omega t + \theta_z$, Ω the speed of rotation imposed to the drillstring, θ_z the twist angle.

2.2. FE drillstring modeling

The drillstring is modeled with 3D Timoshenko beam elements with two nodes (Fig.3), each node containing six degrees of freedom (dof): three translations and three rotations. The beam elements are uniform and homogenous. The elementary displacements $\delta_e = [u, v, w, \theta_x, \theta_y, \theta_z]^T$ are expressed with 12 dofs, the nodal displacements, see Fig.3:

$$\delta_e = N \delta_n \quad (3)$$

135 with $\delta_n = [u_1, v_1, w_1, \theta_{x1}, \theta_{y1}, \theta_{z1}, u_2, v_2, w_2, \theta_{x2}, \theta_{y2}, \theta_{z2}]^T$, N the shape functions matrix. The drillstring equations of motion are established with an energy approach. The application of Lagrange's equation yields the elementary matrices associated with the pipe beam. The calculation of kinematic, strain energies and virtual work of external forces for each element are presented hereafter.

2.2.1. Elementary kinetic energy

Using the instantaneous angular velocity vector in Eq.2, neglecting the higher order terms, and assuming small lateral angles of rotation ($\sin x \approx x$, $\cos x \approx 1$), the classical elementary kinetic energy of drillstring expressed in the

frame of reference (R_1) is:

$$\begin{aligned}
T &= \frac{1}{2}\rho_e S_e \int_0^{l_e} (\dot{u}^2 + \dot{v}^2 + \dot{w}^2) dz + \frac{\rho_e I_e}{2} \int_0^{l_e} (\omega_x^2 + \omega_y^2) dz + \frac{\rho_e I_p^e}{2} \int_0^{l_e} \omega_z^2 dz \\
&= \frac{1}{2}\rho_e S_e \int_0^{l_e} (\dot{u}^2 + \dot{v}^2 + \dot{w}^2) dz + \frac{\rho_e I_e}{2} \int_0^{l_e} (\dot{\theta}_x^2 + \dot{\theta}_y^2) dz + \frac{\rho_e I_p^e}{2} \int_0^{l_e} \dot{\theta}_z^2 dz + \rho_e I_p^e \Omega \int_0^{l_e} \dot{\theta}_x \dot{\theta}_y dz \\
&\quad + \rho_e I_p^e \int_0^{l_e} \Omega \dot{\theta}_z dz + \rho_e I_p^e l_e \Omega^2
\end{aligned} \tag{4}$$

In the expression of T , the first three integrals contribute to the mass matrix due to translation motions, cross-section

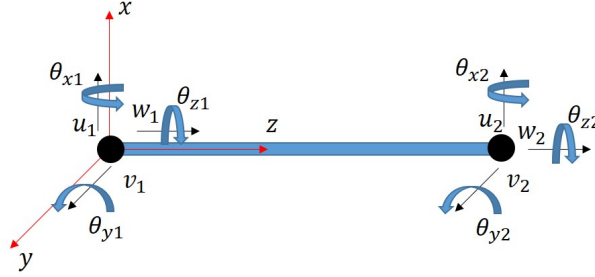


Figure 3: The 6 dofs per node of the beam element

140

inertia, and torsional motion, respectively. The fourth integral represents the gyroscopic effect [21] while the last two terms are eliminated when deriving the Lagrange's equation, due to the drillstring constant speed of rotation Ω .

2.2.2. Elementary strain energy

The elementary strain energy U is composed of the energies associated with the longitudinal, torsional and bending motions, respectively:

$$U = \frac{1}{2} E_e S_e \int_0^{l_e} \left(\frac{\partial w}{\partial z} \right)^2 dz + \frac{1}{2} G_e I_p^e \int_0^{l_e} \left(\frac{\partial \theta_z}{\partial z} \right)^2 dz + \frac{1}{2} E_e I_e \int_0^{l_e} \left[\left(\frac{\partial^2 u}{\partial z^2} \right)^2 + \left(\frac{\partial^2 v}{\partial z^2} \right)^2 \right] dz \tag{5}$$

The stiffness matrix is built by using Eq.5. The shear effect is added into the bending stiffness matrix with the quantity [21]:

$$a = \frac{12 E_e I_e}{G_e S_r^e l_e^2} \tag{6}$$

where S_r^e is the reduced area of the cross-section.

145

2.2.3. Elementary axial - bending coupling

The axial force F_0^e induces stress stiffening. This effect has a primordial role in the case of a slender beam. It is obtained by taking into account the nonlinear quadratic terms of the strain:

$$\epsilon_{zz}^{nl} = \frac{1}{2} \left(\frac{\partial u}{\partial z} \right)^2 + \frac{1}{2} \left(\frac{\partial v}{\partial z} \right)^2 \tag{7}$$

The contribution of the axial force F_0^e is expressed as a strain energy:

$$U_{F_0^e} = \frac{F_0^e}{2} \int_0^{l_e} \left[\left(\frac{\partial u}{\partial z} \right)^2 + \left(\frac{\partial v}{\partial z} \right)^2 \right] dz \tag{8}$$

2.2.4. Elementary torsional - bending coupling

The axial torque T_0^e induces also stress stiffening for any direction of application [22, 23]. As the axial torque is non-conservative, a strain energy can not be established. Its virtual work has to be calculated with its projections in the two bending planes and with the virtual curvatures:

$$\delta W = T_0^e \int_0^{l_e} \left[\frac{\partial v}{\partial z} \delta \left(\frac{\partial^2 u}{\partial z^2} \right) - \frac{\partial u}{\partial z} \delta \left(\frac{\partial^2 v}{\partial z^2} \right) \right] dz \quad (9)$$

2.3. External dynamic forces

2.3.1. Contact forces

150 Under the effects of gravity, external forces and mass unbalance, numerous drillstring borehole contacts occur. Thus, the contact is modelled by three components: normal and tangential contact forces and a friction torque as shown in Fig.4.

The expression of the normal force component is given for example in [24, 25]

$$\mathbf{F}_{cn} = \begin{cases} -(K_c(P)P + C_c(P)\dot{P})\vec{n} & \text{if } P > 0 \\ \vec{0} & \text{if } P \leq 0 \end{cases} \quad (10)$$

with $P = r - j_0$, $r = \sqrt{u^2 + v^2}$, j_0 the drillstring - borehole clearance, $\vec{n} = [u/r, v/r, 0]^T$ the unit normal vector in

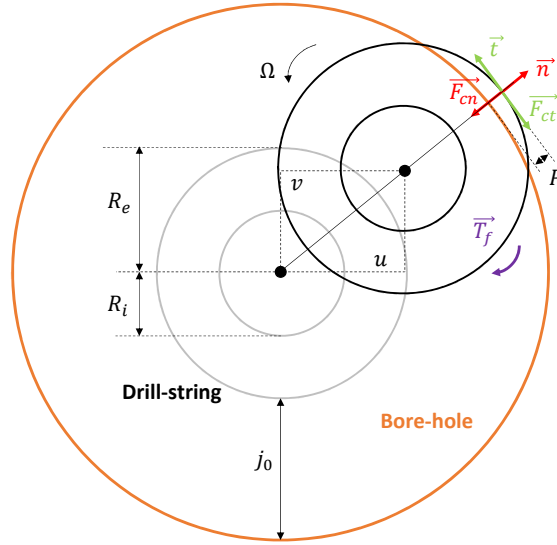


Figure 4: Drillstring borehole interaction

the local frame of reference. The contact stiffness and damping are smoothed by using the arctan function as in [24]:

$$K_c(P) = \frac{k_c}{2} \left[\frac{2}{\pi} \arctan(\pi\lambda_k P) + 1 \right]; C_c(P) = \frac{c_c}{2} \left[\frac{2}{\pi} \arctan(\pi\lambda_c P) + 1 \right] \quad (11)$$

with k_c and c_c the maximum contact stiffness and damping parameters, λ_k and λ_c the regularized parameters. The frictional contact force and torque are calculated by using the Coulomb law:

$$\mathbf{F}_{ct} = -\mu(v_g) |\mathbf{F}_{cn}| \vec{t} \quad (12)$$

$$\mathbf{T}_f = -\mu(v_g) |\mathbf{F}_{cn}| R_e \vec{z} \quad (13)$$

with $\vec{t} = [-v/r, u/r, 0]^T$ the unit tangent vector in the local frame of reference, R_e the outer radius of drillstring. The friction coefficient $\mu(v_g)$ is regularized as a function of the sliding speed v_g of the drillstring on the borehole [24, 25]:

$$\mu(v_g) = \frac{v_g}{2v_{ref}} \left[\frac{1 - \xi}{1 + \frac{(1 - \xi)}{2v_{ref}\mu_d} |v_g|} + \frac{1 + \xi}{\left(1 + \frac{(1 - \xi)}{2v_{ref}\mu_d} |v_g|\right)^2} \right] \quad (14)$$

with $v_g = \frac{u\dot{v} - \dot{u}v}{r} + (\Omega + \dot{\theta}_z) R_e$, $\xi = \sqrt{1 - \frac{\mu_d}{\mu_s}}$, v_{ref} the reference velocity allowing to adjust the slope at zero-speed.

2.3.2. Force due to mass unbalance

The presence of straightness defaults due to the drillstring fabrication and assembly as well as wear or measurement-while-drilling tools [26] possibly makes the drillstring unbalanced. The unbalance is modelled with discrete mass

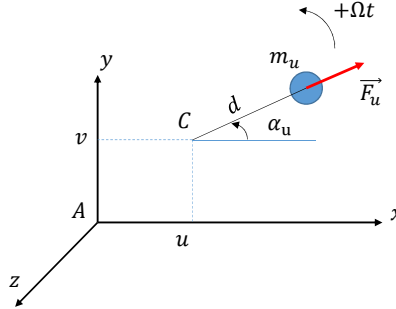


Figure 5: Mass unbalance sketch

unbalances. Let m_u and d be the eccentric mass and gyration radius respectively of one of them [21]. The mass is always in the $x - y$ plane and its initial angular position relative to the x axis is α_u , as shown in Fig.5. Neglecting the angular fluctuation regarding the speed of rotation, the kinetic energy of a discrete mass unbalance at one node in steady state regime is:

$$T_u = \frac{1}{2} m_u d \left[d\Omega^2 - 2\dot{u}\Omega \sin(\Omega t + \alpha_u) + 2\dot{v}\Omega \cos(\Omega t + \alpha_u) \right] \quad (15)$$

which provides through the application of Lagrange's equations the centrifugal force vector $\mathbf{F}_u(t) = [F_u^u, F_u^v, 0, 0, 0, 0]^T$, where:

$$\begin{cases} F_u^u &= m_u d \Omega^2 \cos(\Omega t + \alpha_u) \\ F_u^v &= m_u d \Omega^2 \sin(\Omega t + \alpha_u) \end{cases} \quad (16)$$

155 2.4. Fluid - drillstring interactions

The effects of the fluid flows are modeled by the forces acting on the pipe in the three local directions. The model developed in [13, 16] is adjusted in order to take into account the curved trajectory of the borehole, the eccentricity of annular space due to the deflection of drillstring inside the borehole, and the speed of rotation of the pipe. The detail of the fluid - structure interaction model is presented hereafter.

160 2.4.1. Equations of motion

During the drilling, the filtered fluid is injected downward into the drillpipe with a constant axial speed U_i and then goes back upward into the annular space drillpipe - borehole with a speed U_o conveying rock debris, calories. The pressures inside and outside the drillstring are respectively p_i, p_o and vary linearly along the drillstring. In the undeformed state, the axis of beam element coincides with the center line of borehole. Let dz the length of an element of the drillstring having M_t as mass per unit of length and subject to structural, fluid forces and moments shown in Fig.6. The element is deformed in the plane $r - z$ where r is the radial displacement direction. The forces balance in the z and r directions for one element yield:

$$\begin{cases} 0 = \frac{\partial F_{axial}}{\partial z} + F_{it} - F_{et} - (F_{in} + F_{en})\gamma - \frac{\partial Q}{\partial z} + M_t g \cos \psi \cos \theta \\ 0 = \frac{\partial Q}{\partial z} + (F_{it} - F_{et})\gamma + F_{in} + F_{en} - \frac{\partial F_{axial}\gamma}{\partial z} - M_t a_t \\ -M_t g \sqrt{(-\cos \psi \sin \theta \cos \phi + \sin \psi \sin \phi)^2 + (\cos \psi \sin \theta \sin \phi + \sin \psi \cos \phi)^2} \end{cases} \quad (17)$$

with F_{axial} the axial force, Q the transversal shear force. F_{it}, F_{et} are respectively the tangential forces due to inside and outside fluid flows. F_{in}, F_{en} are respectively the normal forces due to inside and outside fluid flows. a_t is the lateral acceleration of the beam element. γ is the angle between the tangential vectors of the beam center lines in the deformed and undeformed states.

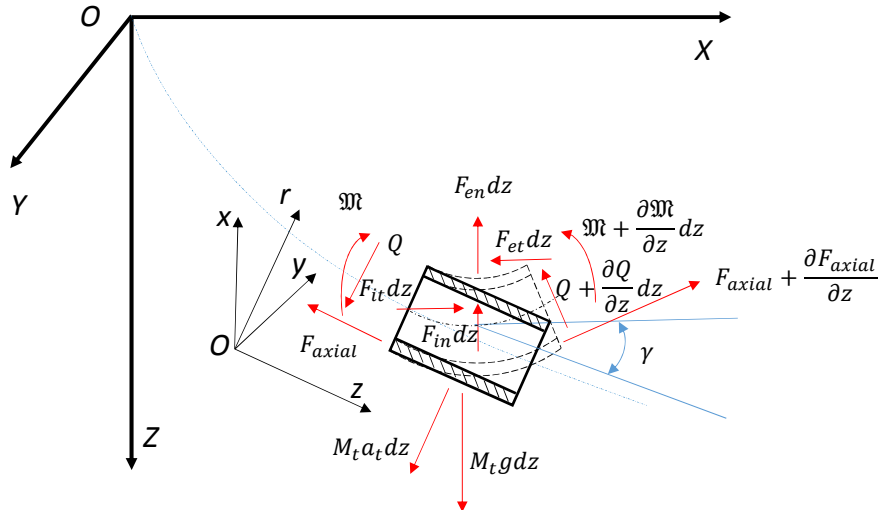


Figure 6: Forces and moments acting on an infinitesimal element of the drillstring

165 2.4.2. Fluid forces due to internal flow

Let the internal fluid element be considered and sketched in Fig.7. The force equilibrium respectively in z and r directions gives:

$$\begin{cases} F_{it} - F_{in}\gamma = -A_i \frac{\partial p_i}{\partial z} + M_f g \cos \psi \cos \theta \\ F_{it}\gamma + F_{in} = -A_i \frac{\partial (p_i \gamma)}{\partial z} - M_f a_f \\ -M_f g \sqrt{(-\cos \psi \sin \theta \cos \phi + \sin \psi \sin \phi)^2 + (\cos \psi \sin \theta \sin \phi + \sin \psi \cos \phi)^2} \end{cases} \quad (18)$$

The accelerations in x, y, z directions of fluid are calculated in [27, 28] assuming that the drillstring is inextensible and the curvature radius of borehole is very important compared to the cross-section radius of the well:

$$\begin{cases} a_{fx} = \frac{\partial^2 u}{\partial z^2} + 2U_i \frac{\partial^2 u}{\partial t \partial z} + U_i^2 \frac{\partial^2 u}{\partial z^2} \\ a_{fy} = \frac{\partial^2 v}{\partial z^2} + 2U_i \frac{\partial^2 v}{\partial t \partial z} + U_i^2 \frac{\partial^2 v}{\partial z^2} \\ a_{fz} = 0 \end{cases} \quad (19)$$

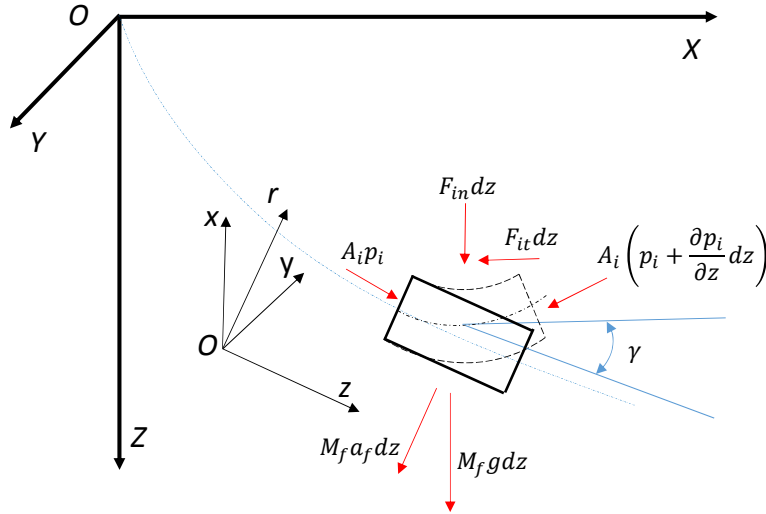


Figure 7: Forces acting on an internal fluid element

2.4.3. Fluid forces due to annular flow

As showed in Fig.8, the beam element is subjected to the forces due to the flow in the annular region. The forces balance in z and r directions gives:

$$\begin{cases} -F_{et} - F_{en}\gamma = -F_L + F_{pz} \\ -F_{et}\gamma + F_{en} = -F_L\gamma - (F_A + F_N) + F_{pr} \end{cases} \quad (20)$$

where fluid forces due to gravity and hydrostatic pressure F_{pz} and F_{pr} are given by:

$$F_{pz} = F_{pX} \sin \theta - F_{pY} \sin \psi \cos \theta - F_{pZ} \cos \psi \cos \theta \quad (21)$$

$$F_{pr} = \sqrt{\left(F_{pX} \cos \theta \cos \phi + F_{pY} (\sin \psi \sin \theta \cos \phi + \cos \psi \sin \phi) - F_{pZ} (-\cos \psi \sin \theta \cos \phi + \sin \psi \sin \psi) \right)^2 + \left(-F_{pX} \cos \theta \sin \phi + F_{pY} (-\sin \psi \sin \theta \sin \phi + \cos \psi \cos \phi) - F_{pZ} (\cos \psi \sin \theta \sin \phi + \sin \psi \cos \phi) \right)^2} \quad (22)$$

F_A is the lateral hydrodynamic inviscid force. F_N, F_L are the friction forces due to the annular flow in the normal and axial directions, respectively.

$$F_L = \frac{1}{2} C_f \rho_f D_o U_o^2 \quad (23)$$

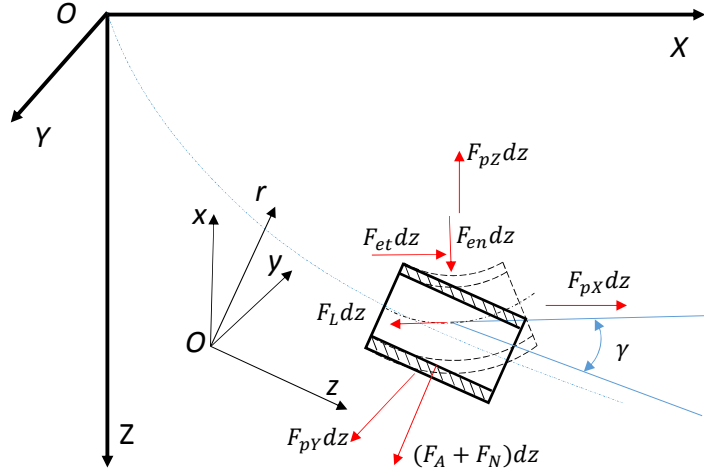


Figure 8: Forces due to annular flow

As the forces F_A and F_N are applied on a drillstring element in the radial direction, their projections along x and y local axes respectively give:

$$F_A^x = \chi \left(\frac{\partial}{\partial t} - U_o \frac{\partial}{\partial z} \right) \left[\rho_f A_o \left(\frac{\partial u}{\partial t} - U_o \frac{\partial u}{\partial z} \right) \right] \quad (24)$$

$$F_A^y = \chi \left(\frac{\partial}{\partial t} - U_o \frac{\partial}{\partial z} \right) \left[\rho_f A_o \left(\frac{\partial v}{\partial t} - U_o \frac{\partial v}{\partial z} \right) \right] \quad (25)$$

$$F_N^x = \frac{1}{2} C_N \rho_f D_o U_o \left(\frac{\partial u}{\partial t} - U_o \frac{\partial u}{\partial z} \right) + k \frac{\partial u}{\partial t} \quad (26)$$

$$F_N^y = \frac{1}{2} C_N \rho_f D_o U_o \left(\frac{\partial v}{\partial t} - U_o \frac{\partial v}{\partial z} \right) + k \frac{\partial v}{\partial t} \quad (27)$$

with A_o the beam cross-section, D_o the external diameter of the beam, ρ_f the fluid density. C_f , C_N , k are the viscous damping coefficients. The first two coefficients are used to take into account the friction fluid - structure in axial and radial directions while the last one, the fluid damping also in lateral direction is related to the rotation of drillstring. In this work, the values of C_f and C_N are extracted from [13]. χ is the added mass coefficient of fluid in the annular space:

$$\chi = \frac{D_{ch}^2 + D_o^2}{D_{ch}^2 - D_o^2} \quad (28)$$

with D_{ch} , the borehole internal diameter. The viscous damping coefficient k is a function of drillstring-borehole geometry, fluid properties and drillstring speed of rotation:

$$k = \frac{2\sqrt{2}}{\sqrt{S}} \left[\frac{1 + \left(\frac{D_o}{D_{ch}} \right)^3}{\left(1 - \left(\frac{D_o}{D_{ch}} \right)^2 \right)^2} \right] \rho_f A_o \Omega \quad (29)$$

with $S = \Omega D_o^2 / 4\nu_f$ the Stokes number. In order to take into account the non Newtonian behavior of the drilling fluid, the viscous damping coefficient C_f is based on [29]. The friction pressure loss of annular fluid flow is estimated considering the eccentricity, the rotation of drillstring inside the borehole and the fluid flow regime by circulating the

Yield-Power-Law fluid in the drilling system. The viscosity in Eq.(29) is estimated by combining the shear rates of axial and tangential fluid flows [30].

The forces related to the gravity and the hydrostatic pressure are calculated based on [31]. The resultant force

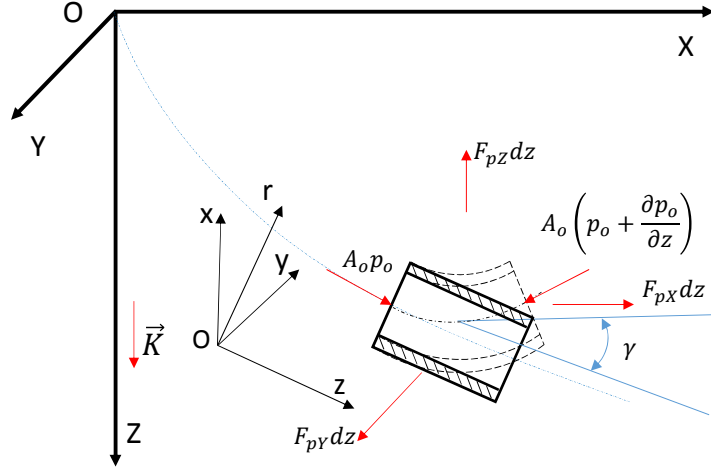


Figure 9: Sketch for calculating forces due to gravity and hydrostatic pressure

applied on the beam element is equal to the buoyancy force in the direction of vector $-\vec{K}$, see Fig.9.

$$\Sigma(\vec{F}_i + \vec{F}_r) = -A_o \frac{\partial p_o}{\partial z} \vec{K} \quad (30)$$

where : \vec{F}_i , \vec{F}_r are respectively resultant forces in the longitudinal and radial directions of drillstring element. The resolution of Eq.30 gives:

$$F_{pz} = A_o \frac{\partial p_o}{\partial z} (1 - \cos \psi \cos \theta) \quad (31)$$

$$F_{pr} = A_o \frac{\partial (p_o \gamma)}{\partial z} - A_o \frac{\partial p_o}{\partial z} \sqrt{\frac{(-\cos \psi \sin \theta \cos \phi + \sin \psi \sin \phi)^2 + (\cos \psi \sin \theta \sin \phi + \sin \psi \cos \phi)^2}{}} \quad (32)$$

2.4.4. Equations of fluid forces discretized by 3D FE beam

Introducing Eqs.18 and 20 into Eq.17 by considering only the terms associated with the fluid, gives the fluid forces acting on the drillstring:

$$\begin{cases} F_{fz} = -A_i \frac{\partial p_i}{\partial z} + M_f g \cos \psi \cos \theta - F_L + F_{pz} \\ F_{fr} = A_i \frac{\partial (p_i \gamma)}{\partial z} + M_f a_f + F_L \gamma + (F_A + F_N) - F_{pr} \end{cases} \quad (33)$$

The substitutions of Eqs.19, 23-27, 31, 32 into Eq.33 with the projection of radial fluid force along x and y

175 directions give the equations of fluid forces acting on a 3D FE beam in local frame:

$$\left\{ \begin{array}{l} F_{fx} = (M_f + \chi\rho_f A_o) \frac{\partial^2 u}{\partial t^2} + \left(\frac{1}{2} C_f \rho_f D_o U_o + k \right) \frac{\partial u}{\partial t} + (2M_f U_i - 2\chi\rho_f A_o U_o) \frac{\partial^2 u}{\partial t \partial z} \\ \quad + (M_f U_i^2 + \chi\rho_f A_o U_o^2 + A_i p_i - A_o p_o) \frac{\partial^2 u}{\partial z^2} + \left(A_i \frac{\partial p_i}{\partial z} - A_o \frac{\partial p_o}{\partial z} \right) \frac{\partial u}{\partial z} \\ \quad - M_{fg} (-\cos \psi \sin \theta \cos \phi + \sin \psi \sin \phi) + A_o \frac{\partial p_o}{\partial z} (-\cos \psi \sin \theta \cos \phi + \sin \psi \sin \phi) \\ F_{fy} = (M_f + \chi\rho_f A_o) \frac{\partial^2 v}{\partial t^2} + \left(\frac{1}{2} C_f \rho_f D_o U_o + k \right) \frac{\partial v}{\partial t} + (2M_f U_i - 2\chi\rho_f A_o U_o) \frac{\partial^2 v}{\partial t \partial z} \\ \quad + (M_f U_i^2 + \chi\rho_f A_o U_o^2 + A_i p_i - A_o p_o) \frac{\partial^2 v}{\partial z^2} + \left(A_i \frac{\partial p_i}{\partial z} - A_o \frac{\partial p_o}{\partial z} \right) \frac{\partial v}{\partial z} \\ \quad - M_{fg} (\cos \psi \sin \theta \sin \phi + \sin \psi \cos \phi) + A_o \frac{\partial p_o}{\partial z} (\cos \psi \sin \theta \sin \phi + \sin \psi \cos \phi) \\ F_{fz} = -A_i \frac{\partial p_i}{\partial z} + M_{fg} \cos \psi \cos \theta - \frac{1}{2} C_f \rho_f D_o U_o^2 - A_o \frac{\partial p_o}{\partial z} (1 - \cos \psi \cos \theta) \end{array} \right. \quad (34)$$

The FE discretization of Eq.(34) gives the mass, stiffness and damping matrices associated with the drilling fluid. The expressions of these matrices are presented in Appendix.

3. Numerical methods for computing the nonlinear response

180 This section presents the nonlinear responses computation of the drillstring taking the drilling fluid effects into account. The assembly yields the FE model and therefore a set of n equations of the fluid - drillstring system described by n dofs inside the borehole. Firstly, the quasi-static equilibrium position of the drillstring is calculated. Then, its transient dynamics inside the borehole is studied.

3.1. Quasi-static equilibrium position

The calculated quasi-static position considers the drillstring contact forces as well as the WOB and TOB developed by the drill bit during the drilling operation. The equilibrium equation is written as:

$$(\mathbf{K} + \mathbf{K}_f) \boldsymbol{\delta} = \mathbf{F}_s + \mathbf{F}_c^{qs}(\boldsymbol{\delta}) \quad (35)$$

with \mathbf{K} the drillstring stiffness matrix including in particular the WOB and TOB stress stiffening effects, \mathbf{K}_f the mud stiffness matrix. The force vector \mathbf{F}_s contains the body forces (gravity and buoyancy), the fluid forces expressed by Eqs. A.4-A.6, the WOB and TOB forces. The quasi-static contact load vector \mathbf{F}_c^{qs} consists of three components: the normal force \mathbf{F}_{cn}^{qs} , the tangential force \mathbf{F}_{ct}^{qs} , and the frictional torque \mathbf{T}_f^{qs} defined by:

$$\left\{ \begin{array}{l} \mathbf{F}_{cn}^{qs} = -K_c(P) P \vec{n} \\ \mathbf{F}_{ct}^{qs} = -\mu_s |\mathbf{F}_{cn}^{qs}| \vec{t} \\ \mathbf{T}_f^{qs} = -\mu_s |\mathbf{F}_{cn}^{qs}| R_e \vec{z} \end{array} \right. \quad (36)$$

185 where μ_s is the static friction coefficient. Eq.35 is solved using a Newton-Raphson method as explained in [32]. It provides the quasi-static position of the drillstring inside the borehole.

3.2. Transient dynamics computation

The nonlinear dynamic behavior of the fluid - drillstring system inside a 3D borehole is governed by the set of n differential equations:

$$(\mathbf{M} + \mathbf{M}_f) \ddot{\boldsymbol{\delta}} + (\mathbf{C} + \mathbf{C}_f) \dot{\boldsymbol{\delta}} + (\mathbf{K} + \mathbf{K}_g + \mathbf{K}_f) \boldsymbol{\delta} = \mathbf{F}_s + \mathbf{F}_c(\dot{\boldsymbol{\delta}}, \boldsymbol{\delta}, t) + \mathbf{F}_u(t) \quad (37)$$

with M , K the classical mass and stiffness matrices, K_g the geometric stiffness matrix due to the initial displacement of the drillstring given by the quasi-static equilibrium calculation. The matrix $C = C^{cor} + C^{damp}$ is composed of the Coriolis and structural damping matrices. The structural damping is given by $C^{damp} = \alpha M + \beta (K + K_g)$, with α and β the Rayleigh coefficients. The presence of fluid induces M_f , C_f and K_f , the added mass, damping, stiffness matrices, respectively. The contact force $F_c(\delta, \delta, t)$ and the mass unbalance force $F_u(t)$ are obtained from section 2.3. Eq.37 is solved by means of a fourth order Runge-Kutta scheme with an adaptative time step [33].

4. Simulation in time domain

4.1. Test case

In order to simulate a realistic drilling dynamic behavior in operation, a 200 m drillstring confined in a 3D well is considered. Figure 10 shows the curved borehole trajectory in global coordinates.

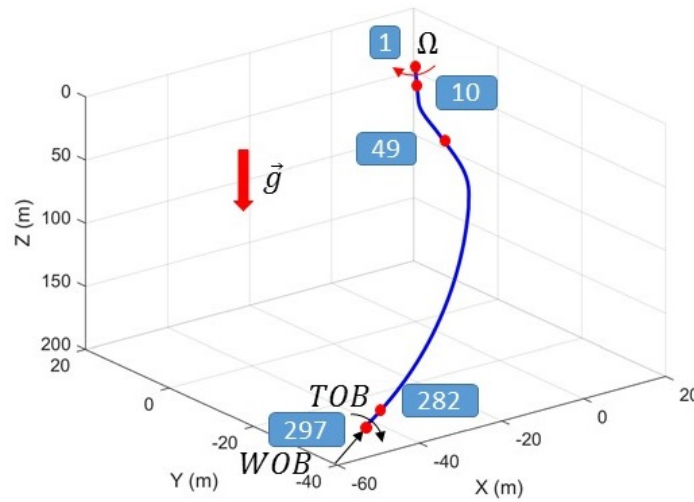


Figure 10: 3D well trajectory

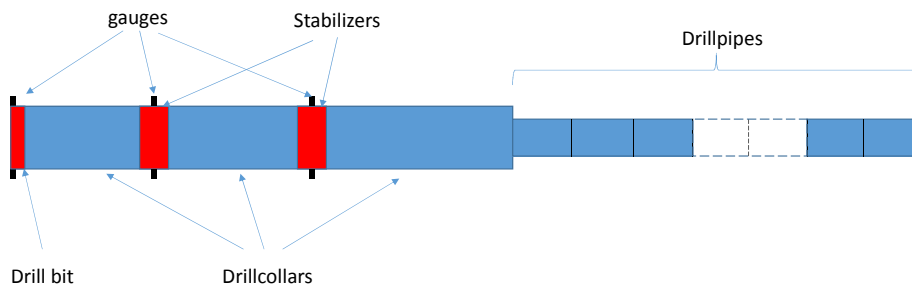


Figure 11: Drillstring assembly

The drillstring is an assembly of pipes with different diameters. It consists of drillpipes, drillcollar, stabilizers, drill bit, see Table.1 and Fig.11. A drillpipe is described in details by Fig.12 and Table.2. The borehole is made of only one open-hole described in Table.3 **In practice, the drillstring-borehole contacts are often located at the tool-joints and**

Table 1: Drillstring composition

Component	Inner diameter (m)	Outer diameter (m)	Curvilinear coordinates s (m) of the gauges	Length (m)
Drillpipe	0.108	0.127	-	89.5
Drillcollar	0.071	0.159	-	33
Stabilizer	0.071	0.159	123.5	2
Drillcollar	0.071	0.159	-	40
Stabilizer	0.071	0.159	165.5	2
Drillcollar	0.071	0.159	-	33
Bit	-	-	200	0.5
Total length (m)				200

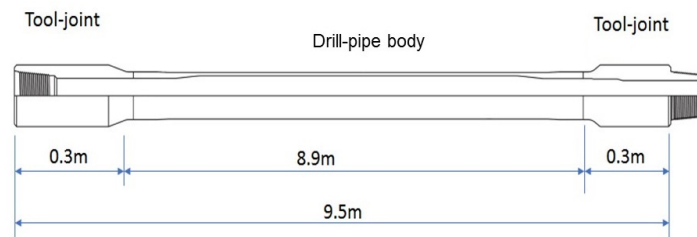


Figure 12: Drillpipe

Table 2: Drillpipe dimensions

Length (m)	Inner diameter (m)	Outer diameter (m)	Tool-joint length (m)	Tool-joint inner diameter (m)	Tool-joint outer diameter (m)
9.5	0.108	0.127	0.3	0.0953	0.1619

Table 3: Borehole description

Description	Drilling diameter (m)	Outer diameter (m)	Inner diameter (m)	Initial measured depth (m)	Shoe depth (m)
Open-hole	0.2159	-	0.2159	0	200

Table 4: Solid and fluid properties

Young modulus	E (N/m ²)	2.03E11
Drillstring density	ρ (kg/m ³)	7900
Poisson's coefficient	ν	0.3
Fluid density	ρ_f (kg/m ³)	1200
Yield stress	τ_y (Pa)	0.29
Consistent index	K (Pa.s ^{n})	0.07
Flow behavior index	n	0.55
Flow rate	Q (m ³ /s)	1E-2

Table 5: Contact modeling parameters

Stiffness	k_c (N/m)	1E7
Damping	c_c (Ns/m)	1E4
Regularized parameters	λ_k, λ_c (m ⁻¹)	7E7, 7E4
Static frictional coefficient	μ_s	0.3
Dynamic frictional coefficient	μ_d	0.2
Regularized frictional	v_{ref} (m/s)	0.033
Rayleigh damping coefficient	α (s ⁻¹)	0.03
Rayleigh damping coefficient	β (s)	0

at the drillcollars. In some cases, contacts can occur at the drillpipe body. Therefore, in this study, the authors used a FE model with element lengths of 30 cm for the tool-joint, 178 cm for the drillpipe body and 25 cm for the drillcollar. With regards to the simulations carried out with different element sizes (not presented in this article), these retained element sizes permit reaching a satisfactory level of accuracy for the static computation and for the dynamic results in the target frequency range. The complete FE drillstring model contains 296 beam elements, and 297 nodes i.e. 1782 dofs. It should be mentioned that the first node at the top of the drillstring is located at the middle of the drillpipe i.e. at its body. Since the drill bit, the stabilizers and the borehole have the same diameter, three gauges reduce the radial clearance to 10⁻⁴ m at the lowest node (drill bit) and at the center of stabilizers in the FE model.

The speed of rotation Ω is imposed at the top of drillstring. By assumption, the elementary gyroscopic matrix is considered constant all along the drillstring. The fluid is pumped downward inside the pipe and upward in the annular space with the mean axial velocities U_i and $-U_o$ respectively and is modelled with the Yield-Power-Law as in [30, 29, 34, 35, 36]. During the rotation, a constant force WOB=-10⁵ N and a constant torque TOB=-5000 Nm are applied to the drill bit. The drillstring material and fluid properties are given in Table 4, and pipe - borehole contacts and structural damping parameters in Table 5.

4.2. Quasi-static position

Figure13 shows the quasi-static equilibrium position of the drillstring. Under the effects of gravity, of fluid and contact forces, the drillstring is bent out of plane. The lateral displacements u and v are not nil for almost all the nodes along the drillstring as shown in Fig.13(a). The radial displacement of each node $r = \sqrt{u^2 + v^2}$ is plotted in Fig.13(b). It shows that the pipe - borehole contacts are located at tooljoints and at almost all the drillcollars.

As shown in Fig.13(b), the drillstring deflects inside the borehole. The pipe - borehole annular space is no longer concentric. This modifies the annular frictional pressure loss characterized by the viscous damping coefficient C_f and generates variable frictional coefficients along the drillstring length. The coefficient C_f , based on the procedure described in [29], is plotted in Fig.14(a). Based on [30], an apparent drilling fluid kinematic viscosity ν_f that combines the fluid flows in the longitudinal and circumferential directions is applied. Thus, the fluid viscosity has a non-constant value, see Fig.14(b).

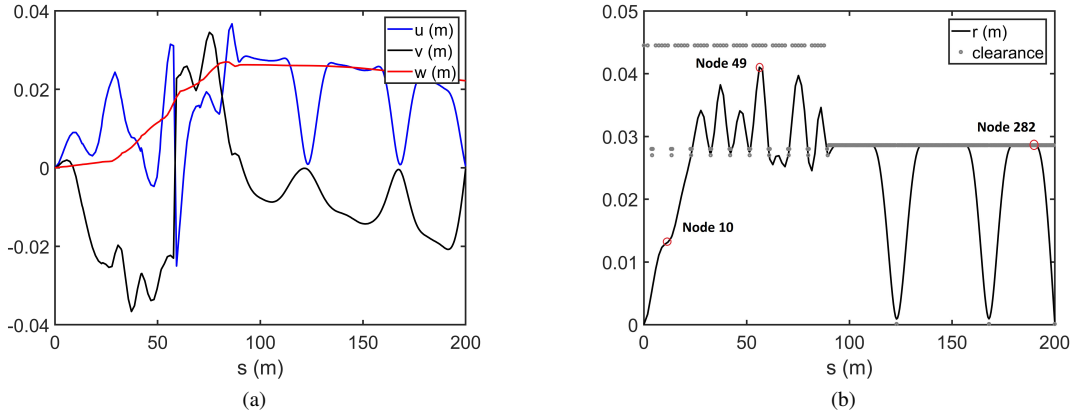


Figure 13: Quasi-static position of drillstring: (a) longitudinal and lateral displacements, (b) radial displacement

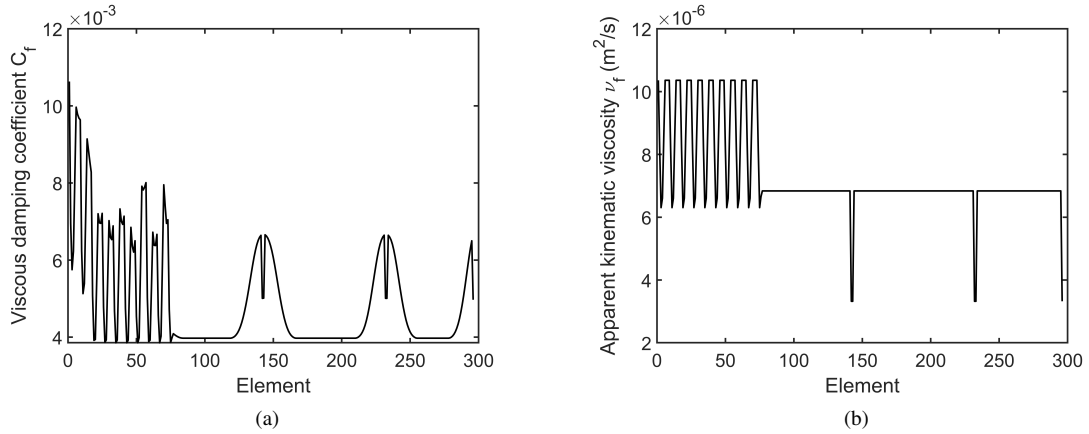


Figure 14: Drilling fluid parameters calculation at each finite element: (a) viscous damping coefficient C_f , (b) apparent kinematic viscosity ν_f

225 4.3. Mass unbalance responses

In this section, the dynamic responses of the drillstring under mass unbalance excitation is studied. In [14, 37, 16] as well as in a previous work of the authors [38], the viscous damping coefficient C_f was considered constant. This means that the pipe - borehole annular space is assumed to be concentric. This is not true in practice since most of the drillstring is in contact with the borehole as shown in Fig.13. Therefore, the computation has to be carried out with the variable viscous damping coefficient and fluid viscosity obtained in the previous quasi-static position calculation, see Fig.14. The mass unbalance related data is calculated based on the 1995 edition of the American Petroleum Institute standards as mentioned in [21]:

$$M_u = \frac{2 \times 6350 \times M_d}{\Omega} \quad (38)$$

with M_u the total mass unbalance (g.mm), M_d the drillstring total mass (kg). The drillstring speed of rotation is assumed to be constant in the mass unbalance forces. The mass unbalance is divided into 17 quantities located along the length of the drillstring and all of them are in phase. The unbalance masses of the drillpipes and the drillcollars are distributed according to their contributions to the drillstring total mass, see Table 6.

230 After the static equilibrium position calculation, almost all the lower part of drillstring is in contact with the borehole wall due to the gravity effect except the nodes near the drill bit and stabilizers gauges. The response of the nodes of this drillstring part could not be destabilized too much as the unbalanced masses are too small compared with

Table 6: Mass unbalance

Location	m_u (kg)	d (m)	α_u (deg)
tooljoints	1.6	0.064	0
drillcollars	1.8	0.058	0

235

the drillcollar mass. Contrary, the drillpipe has only tooljoints contacts. There are some nodes located at the drillpipe body which might have contacts during the dynamic computation because of their important static deflections and to the slenderness of drillpipe i.e. Node 49. In order to have a general observation about the dynamic behavior at several locations along the drillstring, the unbalanced mass response of Nodes 10, 49, and 282 have been considered, as shown in Fig.15.

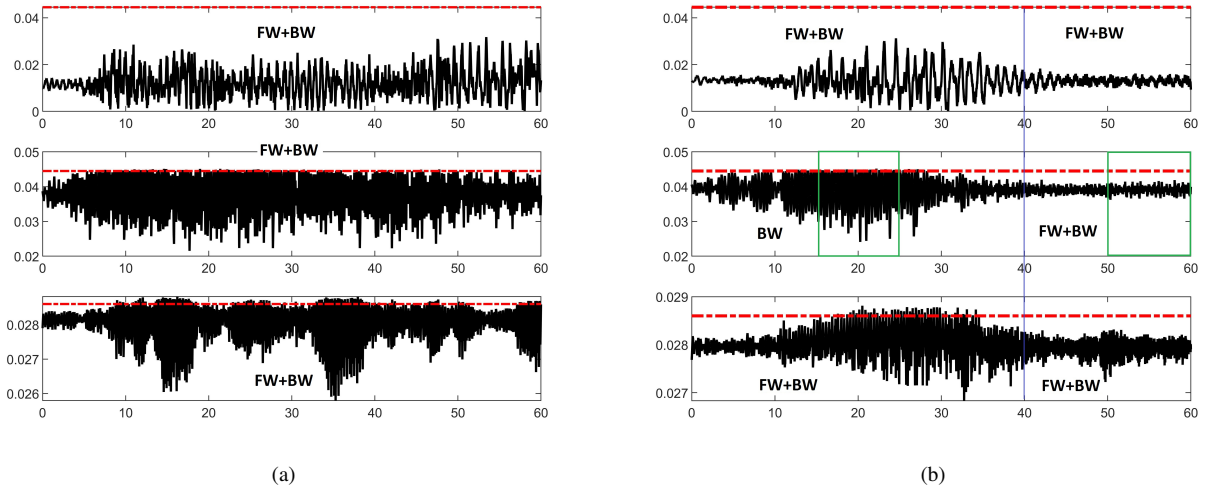


Figure 15: Radial displacement at the Nodes 10 (first row subfigures), 49 (second row subfigures, 282 (third row subfigures): without fluid (a), with fluid (b). The red dashed lines represent the drillstring-borehole clearances. The abscissa is the simulated time [s] while the coordinate is the displacement amplitude [m].

240

245

250

Figure 15 shows the time history radial displacements of Nodes 10, 49, 282. Without fluid, Node 10 located near the drilling surface ($s=11.72$ m) has no contact with the borehole during the 60 s of simulation. Intermittent contacts are observed at Node 49 located on a drillpipe body ($s=57.36$ m) with large bouncing amplitude. Much more number of contacts can be found at Node 282 with important penetration of the drillpipe due to the heavy weight of drillcollar. A quasi-periodic behavior is noticed. The presence of drilling fluid with its damping effect reduces the vibration amplitudes of all considered nodes. A steady state is established roughly after 40 s of simulation. A full spectrum analysis proves the nodes whirl. As shown in Fig.15, the drillstring orbit combines forward and backward whirls in the case without fluid. When the drillstring rotates in drilling fluid, the same observations are noticed at Nodes 10 and 282. However, two different states of vibration occur at Node 49. In the [0 s, 40 s] transient state, Node 49 shows a backward whirl while in the steady state, up to 40 s, it adopts the similar behavior of the other nodes. In order to clarify the fluid effect on the drillstring dynamics, the analysis focuses on the dynamic response at Node 49 in the transient zone [15 s, 25 s], see Fig.16, and in the steady state zone [50 s, 60 s], see Fig.17. The grey circles represent the drillstring-borehole clearance. With no fluid, the lift-off motion from the wellbore which leads to intermittent contacts is noticed, see Fig.16 (a). The full spectrum permits determining the combination of forward or backward whirls in relation to the drillstring rotation [39]. In the field of drilling, the spectral analysis in the [-20 Hz, 20 Hz] ensures the coverage of the operating speed of rotation i.e [60 rpm, 200 rpm]. With no fluid the ± 3.532 Hz peaks are noticeable: the slight difference of their amplitudes can be observed showing that there is no predominant whirling

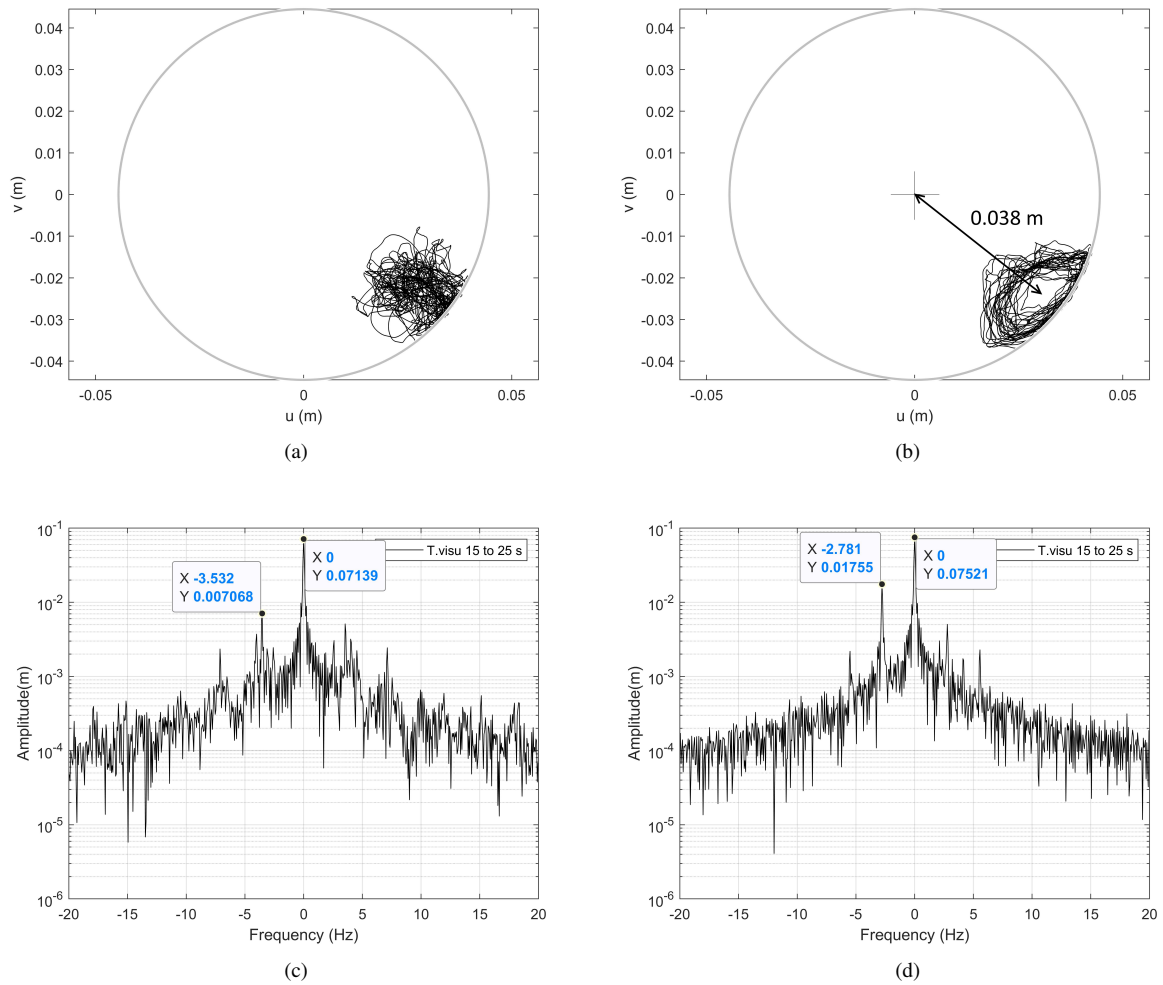


Figure 16: The Node 49 orbits (a, b) and the associated full spectrum analyses (c, d) at the [15 s, 25 s] range: without fluid (a, c), with fluid (b, d).

255 either forward or backward, see Fig.16(c). The fluid forces change the drillstring dynamics as shown in Fig.16 (b, d). Whirling-motions are well noticed. The average offset of orbital center related to the borehole center is about 0.038 m corresponding to half peak amplitude at 0 Hz i.e. 0.07521 m. The -2.781 Hz peak is the most important in the full spectrum plot: the Node 49 orbit has mainly a backward whirl in the [15 s, 25 s] interval. In practice, -2.781 Hz $\approx 32/23\Omega$ peak means that there are 32 main contacts during 23 revolutions of drillstring. As the drillstring runs at 120 rpm, 23 revolutions are done in the last 11.5 seconds of simulation. Figure 18 represents the contact force at Node 49 in the [14.5 s, 26 s] time interval. The main 32 peaks correspond to the main 32 drillstring-borehole contacts. The fluid effect on the drillstring dynamics is also observed through the reduction of the most important frequency in full spectrum analysis from -3.532 Hz to -2.781 Hz. This reduction of vibration frequency is a well-known phenomenon in drillstring modal analysis due to the added mass of drilling fluid [16]. Figure 17 shows that Node 49 has a similar behavior related to the previous time interval in both orbital motion and full spectrum analysis with no drilling fluid. However, the number of contacts decreases resulting in a lift-off motion decrease. In Fig.17 (b, d), the fluid damping reduces the drillstring vibration level. Node 49 has a tight orbit vibrating close to the wellbore without contact. No significant peak is noticed in the full spectrum plot except that one at 0 Hz frequency.

260

265

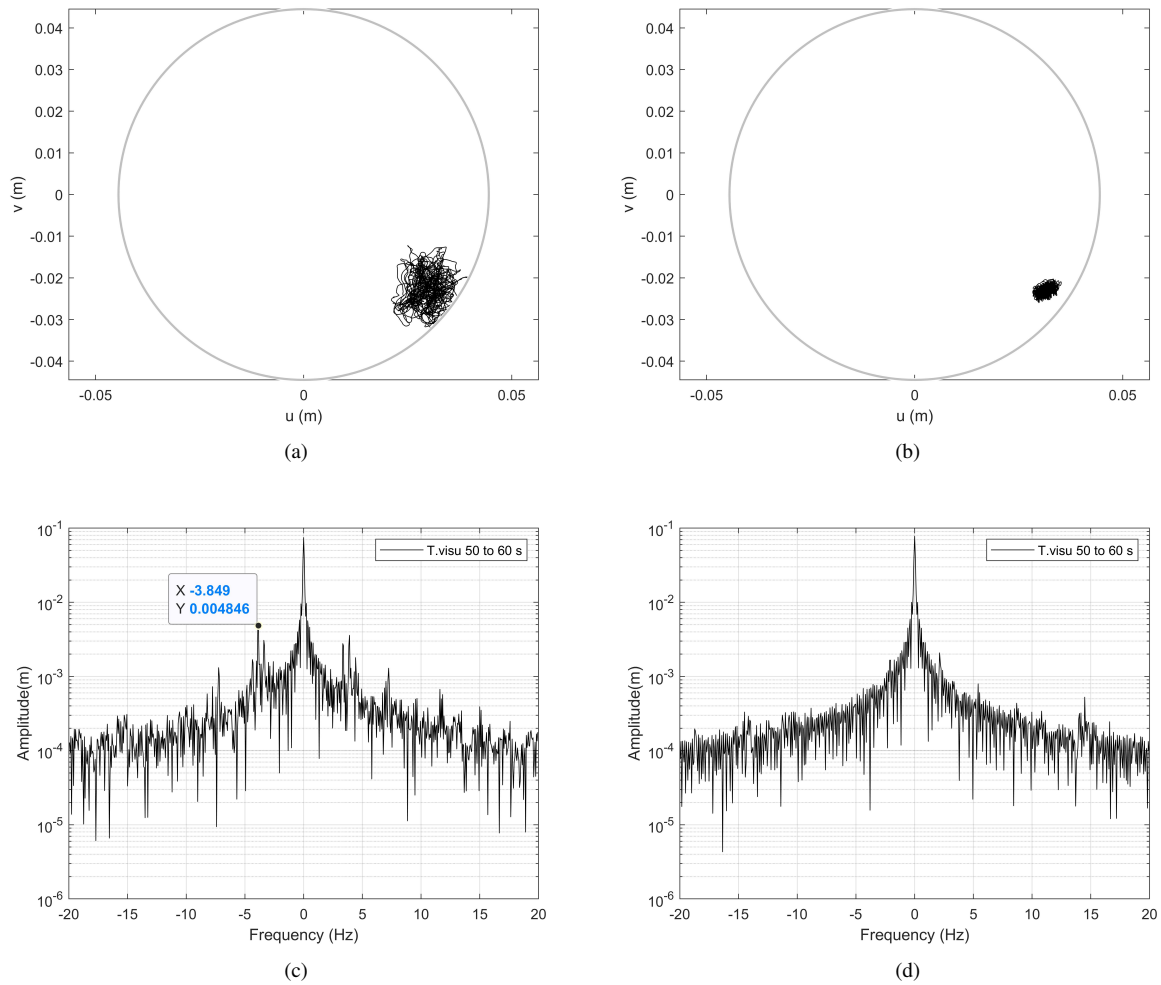


Figure 17: The Node 49 orbits (a, b) and the associated full spectrum analyses (c, d) at the [50 s, 60 s] range: without fluid (a, c), with fluid (b, d).

4.4. Parametric analysis

270 This section is devoted to the influence of some fluid parameters on the mass unbalance response of the drillstring. In the fluid-structure interaction model mentioned in section 2.4, the drilling fluid is assumed to be Yield-Power-Law fluid characterized by consistent index K , yield stress τ_y , and flow behavior index n . Apart from these parameters related to fluid rheology which are fixed for a given fluid, the two other parameters affecting the dynamic behavior are the flow rate Q_f and fluid density ρ_f .

275 4.4.1. Influence of flow rate

280 For this study, the fluid rheology properties are fixed at the values given in Table 4. The flow rate varies from $0.01 \text{ m}^3/\text{s}$ to $0.06 \text{ m}^3/\text{s}$ which are representative flow rates in drilling. Figure 19 (a) compares the Node 49 orbits for several flow rates in [40 s, 60 s] time interval in which a steady state of vibration is established, see Fig.15. The effect of the flow rate is observed. Increasing the flow rate generates more vibrations in terms of orbital motion, this is due to an increase of Reynold's number. In the proposed fluid-structure interaction model, the viscous damping factor is calculated in terms of the Reynold's number which is used to determine the flow regime in the drillstring-borehole annular space. In the $[0.01 \text{ m}^3/\text{s}, 0.06 \text{ m}^3/\text{s}]$ range, the flow is considered as laminar i.e. the Reynold's number is proportional to the fluid density and to the axial fluid flow speed. Moreover, increasing Reynold's number decreases

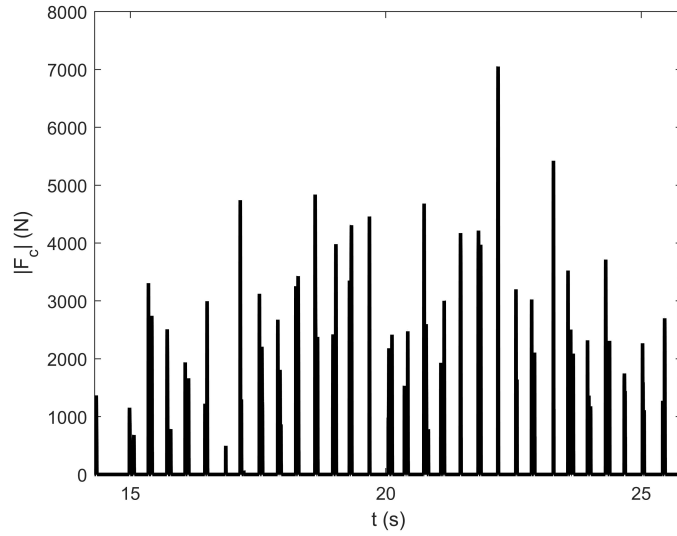


Figure 18: Drillstring-borehole contacts force at Node 49 in the [14.5 s,-26 s] time interval corresponding to 23 simulated revolutions

the fluid viscous damping factor C_f [29], and Fig.20 (a). Therefore, the reduction of fluid damping effect increases the amplitudes of the drillstring vibrations.

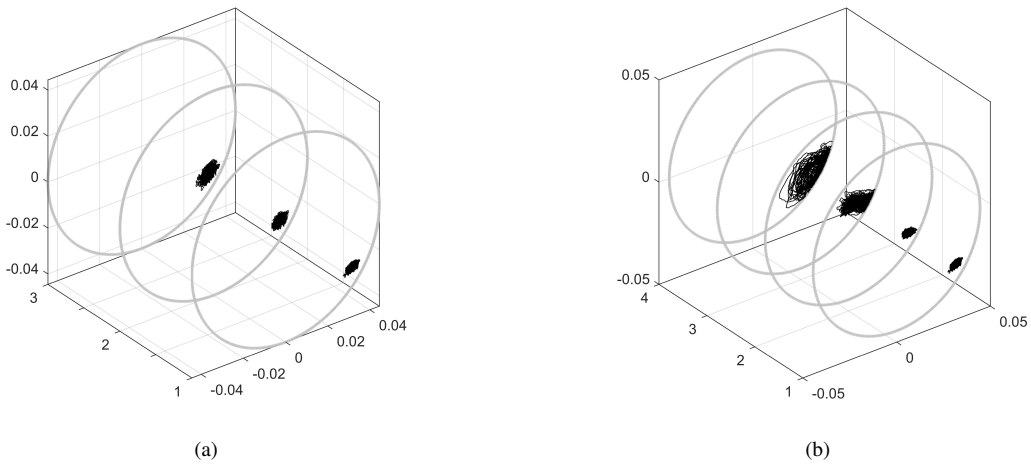


Figure 19: The Node 49 orbits under: (a) flow rate effect - (1) $Q_f=0.01 \text{ m}^3/\text{s}$, (2) $Q_f=0.04 \text{ m}^3/\text{s}$, (3) $Q_f=0.06 \text{ m}^3/\text{s}$; (b) fluid density effect - (1) $\rho_f=1200 \text{ kg}/\text{m}^3$, (2) $\rho_f=1500 \text{ kg}/\text{m}^3$, (3) $\rho_f=1800 \text{ kg}/\text{m}^3$, (4) $\rho_f=2100 \text{ kg}/\text{m}^3$

285

4.4.2. Influences of fluid density

For the parametric study of the fluid density, the other parameters related to drilling fluid are presented in Table 4. In Fig.19 (b), the orbits of Node 49 are plotted for a range of fluid density from $1200 \text{ kg}/\text{m}^3$ to $2100 \text{ kg}/\text{m}^3$ in the [40 s, 60 s] time interval. As discussed previously, increasing the fluid density leads to increase the Reynold's number which reduces the viscous damping factor C_f and then the damping fluid force acting on the drillstring, see Fig.20 (b). However, the fluid densification does not reduce the values of C_f as much as the increase of the flow rate. Furthermore, increasing fluid density provides more inertial force to the drillstring as shown in Eq.34. The apparent influence of

290

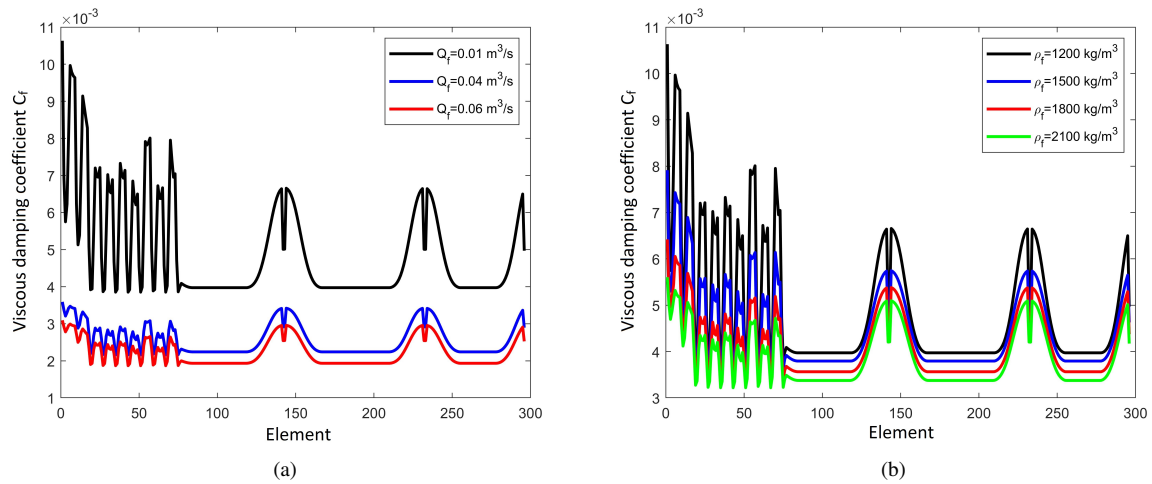


Figure 20: Viscous damping coefficient C_f under: (a) flow rate effect, (b) fluid density effect

fluid density is noticed by analysing the Node 49 orbits under the fluid density effect. A similar behavior is observed when the fluid density increases from 1200 kg/m^3 to 1500 kg/m^3 . Node 49 vibrates always without contact during the time interval considered. But the intermittent contact with higher lift-off motions are noticed when increasing the fluid density to 1800 kg/m^3 . For the most important value of fluid density i.e. 2100 kg/m^3 , Node 49 has a larger orbital motion compared with the other values of fluid density. With the full spectrum analysis (not plotted here), a backward whirl motion is identified for Node 49 when rotating in fluid having a density of 2100 kg/m^3 .

5. Conclusion and remark

The original model presented in this paper is a contribution to the prediction of the dynamic behavior of a rotary drillstring in a 3D curved well subject to fluid-structure interactions, nonlinear forces due to pipe - borehole contact and mass unbalance. The rotation and deflection of the drillstring inside the borehole are considered for the calculation of the viscous damping coefficient and the apparent kinematic viscosity related to drilling fluid. The application concerns an existing 3D-borehole well. The predicted results show the role of the drilling fluid on the drillstring behavior. The drilling fluid reduces the number and the duration of the drillstring borehole contacts, the rebound amplitudes. The carried out parametric analysis highlights that an increase flow rate leads to reduce the fluid damping effect on the drillstring vibration. The same phenomenon is observed when increasing the fluid density. However, this one has a bigger effect on drillstring dynamics than the flow rate effect.

In this work, the drillstring dynamics is simulated under constant values of WOB and TOB. The fluid forces are also assumed to be constant during the dynamic simulation. All of these assumptions help to establish the current model and its computation. In future works, a bit-rock interaction model as well as the fluid forces updated during the dynamic response calculation have to be implemented for making the simulated results more realistic.

Acknowledgment

This research is conducted by Drillab, a joint laboratory of DrillScan and LaMCoS, grant Labcom-SME program ANR 15-LCV4-0010-01. The authors are indebted to the Agence Nationale de la Recherche (ANR) for its financial support.

Appendix. Matrices and force vectors of the fluid

The discretization of Eq.34 by using FE method and beam shape functions in Eq.3 gives the added mass, damping, stiffness elementary matrices and vectors of fluid forces associated to the drilling fluid :

$$[\mathbf{M}_e]^f = \int_0^1 (M_f + \chi\rho_f A_o) (N_u^T(\xi) N_u(\xi) + N_v^T(\xi) N_v(\xi)) l_e d\xi \quad (\text{A.1})$$

$$\begin{aligned} [\mathbf{C}_e]^f &= \int_0^1 \left(\left(\frac{1}{2} C_f \rho_f D_o U_o + k \right) (N_u^T(\xi) N_u(\xi) + N_v^T(\xi) N_v(\xi)) l_e \right) d\xi \\ &+ \int_0^1 (2M_f U_i - 2\chi\rho_f A_o U_o) \left(\left[\frac{\partial N_u(\xi)}{\partial \xi} \right]^T N_u(\xi) + \left[\frac{\partial N_v(\xi)}{\partial \xi} \right]^T N_v(\xi) \right) d\xi \end{aligned} \quad (\text{A.2})$$

$$[\mathbf{K}_e]^f = \int_0^1 \left[\begin{array}{c} (M_f U_i^2 + \chi\rho_f A_o U_o^2 + A_i p_i - A_o p_o) \\ \left(\left[\frac{\partial^2 N_u(\xi)}{\partial \xi^2} \right]^T N_u(\xi) + \left[\frac{\partial^2 N_v(\xi)}{\partial \xi^2} \right]^T N_v(\xi) \right) \frac{1}{l_e} \\ + \left(A_i \frac{\partial p_i}{\partial z} - A_o \frac{\partial p_o}{\partial z} \right) \left(\left[\frac{\partial N_u(\xi)}{\partial \xi} \right]^T N_u(\xi) + \left[\frac{\partial N_v(\xi)}{\partial \xi} \right]^T N_v(\xi) \right) \end{array} \right] d\xi \quad (\text{A.3})$$

$$\mathbf{f}_f^x = \int_0^1 \left[\begin{array}{c} M_f g (-\cos \psi \sin \theta \cos \phi + \sin \psi \sin \phi) \\ -A_o \frac{\partial p_o}{\partial z} (-\cos \psi \sin \theta \cos \phi + \sin \psi \sin \phi) \end{array} \right] N_u^T(\xi) l_e d\xi \quad (\text{A.4})$$

$$\mathbf{f}_f^y = \int_0^1 \left[\begin{array}{c} M_f g (\cos \psi \sin \theta \sin \phi + \sin \psi \cos \phi) \\ -A_o \frac{\partial p_o}{\partial z} (\cos \psi \sin \theta \sin \phi + \sin \psi \cos \phi) \end{array} \right] N_v^T(\xi) l_e d\xi \quad (\text{A.5})$$

$$\mathbf{f}_f^z = \int_0^1 \left[\begin{array}{c} M_f g \cos \psi \cos \theta - A_i \frac{\partial p_i}{\partial z} - \frac{1}{2} C_f \rho_f D_o U_o^2 \\ + A_o \frac{\partial p_o}{\partial z} (1 - \cos \psi \cos \theta) \end{array} \right] N_w^T(\xi) l_e d\xi \quad (\text{A.6})$$

where l_e is the beam element length, $\xi = z/l_e$.

References

- 320 [1] Y. A. Khulief, F. A. Al-Sulaiman, S. Bashmal, Vibration analysis of drillstrings with self-excited stick-slip oscillations, *Journal of Sound and Vibration* 299 (2007) 540–558.
- [2] H. Melakhessou, A. Berlioz, G. Ferraris, A nonlinear well-drillstring interaction model, *Journal of Vibration and Acoustics* 125 (2003) 46–52.
- [3] M. T. Piovan, R. Sampaio, Nonlinear model for coupled vibrations of drill-strings, *Mécanica Computacional* 25 (2006) 1751–1765.
- 325 [4] A. S. Yigit, A. P. Christoforou, Coupled torsional and bending vibrations of actively controlled drillstrings, *Journal of Sound and Vibration* 234 (2000) 67–83.
- [5] S. S. Chen, M. W. Wambsganss, J. A. Jendrzejczyk, Added mass and damping of a vibrating rod in confined viscous fluids, *Journal of Applied Mechanics* (1976) 326–329.
- [6] R. J. Shuy, Bending vibration of rotating drill strings, Ph.D. thesis, Massachusetts Institute of Technology (1989).
- 330 [7] G. Heisig, Lateral drillstring vibrations in extended-reach wells, in: (SPE Paper 59235) IADC/SPE Drilling Conference and Exhibition, 23–25 February 2000, New Orleans, Louisiana, USA, Society of Petroleum Engineers, 2000.
- [8] V. F. Sinyavskii, Oscillation of a cylinder in a viscous liquid, *Prikladnaya Mekhanika* 16 (1980) 62–67.
- [9] J. A. Axisa, J. Antunes, Flexural vibrations of rotors immersed in dense fluid-Part II: Experiments, *Journal of Fluids and Structures* 6 (1992) 23–38.
- [10] J. A. Axisa, J. Antunes, Flexural vibrations of rotors immersed in dense fluid-Part I: Theory, *Journal of Fluids and Structures* 6 (1992) 3–21.
- 335 [11] J. Antunes, F. Axisa, T. Grunenwald, Dynamics of rotors immersed in eccentric annular flow. Part 1: Theory, *Journal of Fluids and Structures* 10 (1996) 893–918.
- [12] Y. A. Khulief, F. A. Al-Sulaiman (Eds.), Laboratory investigation of drillstring vibrations, Vol. 223, Proceedings of the Institution of Mechanical Engineers, Part C: Journal of Mechanical Engineering Science, 2009.
- 340 [13] M. P. Paidoussis, T. P. Luu, S. Prabhakar, Dynamics of a long tubular cantilever conveying fluid downwards, which the flows upwards around the cantilever as a confined annular flow, *Journal of Fluids and Structure* 24 (2008) 111–128.

- [14] A. A. Jafari, R. Kazemi, M. F. Mahyari, The effects of drilling mud and weight bit on stability and vibration of a drill string, *Journal of Vibration and Acoustics* 134 (1) (2011) 1–9.
- [15] Y.-C. Pei, Y.-H. Sun, J.-X. Wang, Dynamics of rotation conveying mud drill string subjected to torque and longitudinal thrust, *Meccanica* 48 (2013) 2189–2201.
- 345 [16] T. G. Ritto, C. Soize, R. Sampaio, Nonlinear dynamics of a drill-string with uncertain model of the bit-rock interaction., *International Journal of Nonlinear Mechanics* 44 (2009) 865–876.
- [17] J. K. Wilson, S. F. Noynaert, A new damping model for nonlinear drillstring dynamics, in: (SPE Paper 178817) IADC/SPE Drilling Conference and Exhibition, 1-3 March, Fort Worth, Texas, USA, Society of Petroleum Engineers, 2016.
- [18] Q. Zhang, S. Miska, E. Kuru, J. J. Azar, Critical flow rate for the buckling of nonrotating drillpipe conveying fluid in vertical holes, in: (SPE Paper 63195) Annual Technical Conference and Exhibition, 1-4 October, Dallas, Texas, Society of Petroleum Engineers, 2000.
- 350 [19] T. Feng, I. Kim, D. Chen, Dynamic modeling of directional drillstring: A linearized model considering well profile, *Journal of Dynamics Systems, Measurement, and Control* 140 (2017) 10.
- [20] T. Feng, S. Bakshi, Q. Gu, D. Chen, A finite element modeling framework for planar curved beam dynamics considering nonlinearities and contacts, *Journal of Computational and Nonlinear Dynamics* 14 (8).
- 355 [21] M. Lalanne, G. Ferraris, *Rotordynamics Prediction In Engineering*, Second Edition, John Wiley and sons, 1998.
- [22] A. Berlioz, J. Der Hagopian, R. Dufour, Dynamic behavior of a drill-string: Experimental investigation of lateral instabilities, *Journal of Vibration and Acoustics* 118 (1996) 292–298.
- [23] R. Dufour, A. Berlioz, Parametric instability of a beam due to axial excitations and to boundary conditions, *Journal of Vibration and Acoustics* 120 (1998) 461–467.
- 360 [24] C. Duran, L. Manin, M.-A. Andrianoely, C. Bordegaray, F. Battle, R. Dufour, Effect of rotor-stator contact on the mass unbalance response, in: 9th IFToMM International Conference on Rotor Dynamics, Proceedings, Milano, IT, Sep 22-25, 2014, Vol. 21, 2014, pp. 1965–1975.
- [25] C. Duran, L. Manin, M.-A. Andrianoely, C. Bordegaray, R. Dufour, An analysis of rotor-stator interaction, in: 10th International Conference on Vibrations in Rotating Machinery (VIRM10), IMechE, London, Sept. 2012, London, United Kingdom, 2012.
- [26] P. D. Spanos, A. M. Chevallier, N. P. Politis, M. L. Payne, Oil and gas well drilling: A vibrations perspective, *Shock & Vibration Digest* 35 (2) (2003) 85.
- 365 [27] Q. Ni, M. Tang, Y. Wang, L. Wang, In-plane and out-of-plane dynamics of a curved pipe conveying pulsating fluid, *Nonlinear Dynamics* 75 (2014) 603–619.
- [28] M. P. Paidoussis, *Fluid-structure interactions - slender structures and axial flow*, Vol. 1, Academic Press, 1998.
- [29] O. Erge, E. M. Ozbayoglu, S. Miska, M. Yu, N. Takach, A. Saasen, R. May, The effects of drillstring eccentricity, rotation, and buckling configurations on annular frictional pressure losses while circulating Yield Power Law fluids, in: (SPE Paper 167950) IADC/SPE Drilling Conference and Exhibition, 4-6 March, Fort Worth, Texas, USA, Society of Petroleum Engineers, 2014.
- 370 [30] R. Ahmed, S. Miska, Experimental study and modelling of Yield Power Law fluid flow in annuli with drillpipe rotation, in: (SPE Paper 59235) IADC/SPE Drilling Conference and Exhibition, 4–6 March 2008, Orlando, Florida, USA, Society of Petroleum Engineers, 2008.
- [31] M. P. Paidoussis, Dynamics of cylindrical structures subjected to axial flow, *Journal of Sound and Vibration* 29 (1973) 365–385.
- 375 [32] K.-L. Nguyen, Q.-T. Tran, M.-A. Andrianoely, L. Manin, S. Menand, R. Dufour, A rotordynamics model for rotary drillstring with nonlinear interactions in a 3D well, in: *Mechanisms and Machine Science*, Vol. 62, Springer Netherlands, 2019.
- [33] K.-L. Nguyen, Q.-T. Tran, L. Manin, S. Baguet, M. A. Andrianoely, L. Piau, R. Dufour, Un schéma d’intégration temporelle pour la réponse transitoire de systèmes mécaniques avec butées de contact (A time integration scheme for transient dynamic response of mechanical oscillator with stop-ends) (in French), in: 23ème Congrès Français de Mécanique [CFM2017], Lille, France, 2017.
- 380 [34] O. Erge, M. E. Ozbayoglu, S. Miska, M. Yu, N. Takach, A. Saasen, R. May, Effect of drillstring deflection and rotary speed on annular frictional pressure losses, *Journal of Energy Ressources Technology* 136 (2014) 10.
- [35] O. Erge, M. E. Ozbayoglu, S. Miska, M. Yu, N. Takach, A. Saasen, R. May, CFD analysis and model comparison of annular frictional pressure losses while circulating Yield Power Law fluids, in: (SPE Paper 173840) SPE Bergen One Day Seminar, 22 April, Bergen, Norway, Society of Petroleum Engineers, 2015.
- 385 [36] O. Erge, A. K. Vajargah, M. E. Ozbayoglu, E. V. Oort, Frictional pressure loss of drilling fluids in a fully eccentric annulus, *Journal of Natural Gas Science and Engineering* 26 (2015) 1119–1129.
- [37] H. Qiu, J. Yang, S. Butt, J. Zhong, Investigation on random vibration of a drillstring, *Journal of Sound and Vibration* 406 (2017) 74–88.
- [38] Q.-T. Tran, K.-L. Nguyen, L. Manin, M.-A. Andrianoely, S. Baguet, S. Menand, R. Dufour, Nonlinear dynamics of a rotary drill-string immersed in a 3D geometry well, in: *Mechanisms and Machine Science*, Vol. 63, Springer Netherlands, 2019, pp. 265–279.
- 390 [39] P. Goldman, A. Muszynska, Application of full spectrum to rotating machinery diagnostics, *Orbit* 20 (1) (1999) 17–21.